Characterising Hot Subdwarf Stars from the Sloan Digital Sky Survey

A report submitted as a component to the degree of
Bachelor of Science

by

Simon Hall

Armagh Observatory
Armagh, Northern Ireland

&

School of Physics

Faculty of Engineering, Mathematics and Science
University of Dublin, Trinity College
Dublin, Ireland

December 2008

Acknowledgements

I would like to sincerely thank my supervisor, C.S. Jeffery, for providing me with a research topic for my final year project, and for his patience, advice and assistance throughout.

I am very grateful to Chris Winter, who supplied me with the code necessary to conduct this research, and who provided every assistance when required, which was often.

I should write a quick note of thanks to the SDSS team and participating institutions for providing all of the data used during the course of this project.

I would like also to mention the staff and students at Armagh Observatory for their friendly welcome, provision of a wonderful working environment and their helpful support. Special thanks to Toby, Eamonn and Geert, who put a roof over my head for 3 months.

Lastly, but by no means leastly, I would like to thank my parents, family and friends for their continued support, both financial and, well, non-financial.

Simon Hall

Created with LaTeX

Abstract

The aim of this project is to classify and parameterise a large sample of stellar spectra, namely those of hot subdwarf stars included in the most recent data release from the Sloan Digital Sky Survey (SDSS). This will be achieved by making use of a number of automatic analysis techniques developed by Winter (2006) at Armagh Observatory (1). These include Principal Component Analysis (PCA) to filter for desirable stellar spectra, supervised training of an artificial neural network (ANN) for automated classification and finally parameterisation in terms of $\log g$, effective temperature and helium abundance using a χ^2 fitting algorithm. The results will allow us to examine the distribution of these stars in parameter space with a view to constraining their evolutionary development.

Contents

Acknowledgements i

Abstract ii

List of Tables v

List of Figures vi

1 Introduction 1

1.1 What is a star? . . . 1

1.2 Stellar Evolution . . . 2

1.3 Stellar Properties . . . 3

1.3.1 Effective Temperature . . . 3

1.3.2 Surface Gravity . . . 4

1.3.3 Magnitude . . . 4

1.3.4 Colour . . . 5

1.4 Spectroscopy . . . 6

1.5 Subdwarf Stars . . . 7

2 The Sloan Digital Sky Survey (SDSS) 9

2.1 What is the SDSS? . . . 9

2.2 SDSS Instrumentation . . . 9

2.3 Observational process . . . 10

3 Computational Methods **11**

3.1 Principal Component Analysis 11

3.1.1 Mathematics of PCA 12

3.1.2 Building a hot subdwarf filter 13

3.2 Artificial Neural Network 13

3.3 χ^2 Fitting 14

4 Application to SDSS Hot Subdwarfs **16**

4.1 Search Criteria 16

4.2 Filtering 17

4.3 Analysis 18

4.3.1 Classification 18

4.3.2 Paramaterisation 20

4.4 Error Analysis 23

5 Conclusion **24**

Bibliography **26**

List of Tables

4.1 Range of Classification 19

4.2 LTE Model Grid 20

List of Figures

1.1 HR diagram 2

1.2 A plot showing the band pass intensity curves for the five SDSS filters. . 5

1.3 An example of an SDSS stellar spectrum, resampled between 3800Å and 4950Å. The hydrogen Balmer absorption lines are evident. 7

4.1 The first Principal Component of the Drilling et al. (10) sample. These are the three hydrogen Balmer lines: $H\beta$, $H\gamma$ and $H\delta$. 17

4.2 A plot of Helium Class against Spectral Type. For clarity, points have been offset by small random shifts in both coordinates. 19

4.3 A plot of Luminosity Class against Spectral Type. For clarity, points have been offset by small random shifts in both coordinates. 19

4.4 A plot of Helium Class against Luminosity Class. For clarity, points have been offset by small random shifts in both coordinates. 20

4.5 A plot of Surface Gravity against Effective Temperature. 21

4.6 A plot of Helium Abundance against Effective Temperature. 22

Chapter 1

Introduction

1.1 What is a star?

A star is a massive, luminous ball of plasma - or ionised gas. A star's luminosity is due solely to the outward migration of photons of electromagnetic energy derived from thermonuclear fusion processes within the body of the star itself. When the first stars were forming in the early Universe, the only elements available were those left over from the Big Bang - hydrogen (about 74%), helium (about 25%), and minute traces of other light elements such as deuterium and lithium (2). Thus, the oldest stars condensed within a molecular cloud composed largely of hydrogen. Once a critical mass of material (the so called Jeans mass) accumulates within a certain distance (the Jeans length), the gaseous pressure of the cloud can no longer prevent gravitational collapse (3). Gravitational potential energy is converted to heat as the gas contracts, culminating with the thermonuclear fusion of hydrogen to helium within the core once a threshold temperature has been reached. The pressure exerted by both the gas and the random walk of radiant photons produced as a result of these nuclear reactions is sufficient to counteract further gravitational collapse and equilibrium is established. However, there is a natural upper and lower bound to the mass of these collapsing stars - protostars below about $0.08M_{\odot}$ eventually cool without ever engaging in stellar nucleosynthesis, forming small brown dwarfs. Protostars above about $100M_{\odot}$ manifest themselves as highly unstable Wolf-Rayet stars, unable to gravitationally retain their outer layers.

1.2 Stellar Evolution

A Hertzprung-Russell diagram is a very useful illustration of the relationship between various key stellar properties which we shall examine shortly, namely the luminosity (which is related to the absolute magnitude) and the effective temperature (related to both spectral type and colour) of a range of stars. An example is shown in Figure 1.1.

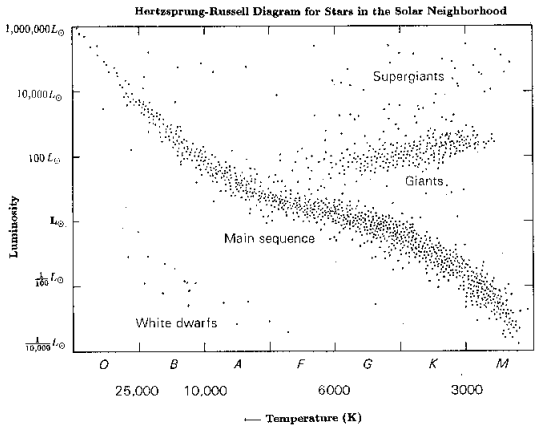

Figure 1.1: Hertzsprung-Russell Diagram: a plot of luminosity (absolute magnitude) against effective temperature (colour) of stars ranging from the high-temperature blue stars on the left side of the diagram to the low-temperature red stars on the right.

The diagram is plotted in such a way that the absolute magnitude increases along the positive vertical axis and the temperature decreases along the positive horizontal axis. Stars at the bottom right are faint, cool and red while stars at the top left are bright, hot and blue. The period of time during which a star is in the process of core hydrogen fusion is called the main sequence (5). This is the principal feature of the Hertzprung-Russell diagram - a large band of stars forming the diagonal sloping downward from left to right. The evolution of a star is determined predominantly by its mass. A very large mass will burn through its supply of hydrogen much faster than a star of average, or small mass. However, once a star has used up all of its core hydrogen, fusion of the lightest element moves to an envelope surrounding the core. This forces the star to expand rather dramatically into a prominent entity known as a red giant. Diagrammatically, the star migrates away from the main sequence and joins the giant branch (5). Depending on mass, a star may begin a phase of core helium burning to still heavier elements, and the star joins the horizontal branch. Eventually, all sources of nuclear fuel (up to and including silicon conversion to iron) are exhausted and a star can no longer maintain equilibrium - the star approaches the end of its life

(3). Large stars typically go out with a bang. Once radiative pressure is relieved, a sufficiently large star will not be able to prevent cataclysmic gravitational collapse to form an extremely dense neutron star or a black hole, a singularity of infinitesimal size containing an enormous amount of mass. Intermediate stars undergo sequences of inward collapse and explosion, releasing huge bursts of gravitational potential energy and expelling a large amount of material into interstellar space, leaving behind a white dwarf supported entirely by electron degeneracy. Still smaller stars probably also end their life as a white dwarf. Not much is known about the evolutionary process of smaller stars as their main sequence can last as long as the Universe has been in existence. After a number of generations of star formation, interstellar space would become 'polluted' with heavier elements - created during nuclear fusion within stars or later through nucleosynthesis during a supernova event. These heavy elements would later form more diverse stars, planets and even people.

1.3 Stellar Properties

There are a number of properties of a star which are of fundamental astrophysical importance. The stellar atmospheric parameters of effective temperature ($T_{\rm eff}$) and surface gravity ($\log g$) are two such values. They are directly related to the physical properties of the star; mass (M), radius (R) and luminosity (L). In addition, the magnitude and colour of the object are important classification tools. Lastly, analysis of the stellar spectrum is an invaluable diagnostic tool, without which many of the above properties would remain elusive.

1.3.1 Effective Temperature

The effective temperature of a star is physically related to the total radiant power per unit area at the stellar surface (F):

$$\sigma T_{\rm eff}^4 \equiv \int_0^\infty F_\nu d\nu = \frac{L}{4\pi R^2} \tag{1.1}$$

This is the temperature that gives the same total power output per unit area as an equivalent blackbody, and is related to both stelar luminosity and radius. There is no true surface to a star, so the stellar radius can vary with wavelength and the nature of the star itself. The radius is generally taken as the depth of formation of the continuum, which in the visible region is approximately constant for most stars (4).

1.3.2 Surface Gravity

The surface gravity of a star is given by the stellar mass and the radius according to Newton's Law of Universal Gravitation. Taking $g_\odot$ in cgs units, and both M and R in solar units, this gives us:

$$g = g_\odot \frac{M}{R^2} \tag{1.2}$$

or, logarithmically,

$$\log g = \log M - 2\log R + \log g_\odot = \log M - 2\log R + 4.437 \tag{1.3}$$

For our Sun, with $R = 1$ and $M = 1$, this gives $\log g = 4.437$. Surface gravity is a measure of the photospheric pressure of the stellar atmosphere.

1.3.3 Magnitude

Magnitude refers to the brightness of an object. The scale upon which magnitude now rests has its origin in the Hellinistic practice of dividing those stars visible to the naked eye into six magnitudes. The brightest corresponding to first magnitude ($m = 1$), while the faintest were of sixth magnitude ($m = 6$). The human eye best differentiates between brightness or flux (F) ratios and as a result, a logarithmic magnitude scale evolved. There are a number of different logarithmic magnitudes: apparent magnitude, m; absolute magnitude, M; and bolometric magnitude, M_B.

For historical reasons, the apparent magnitude is defined such that a ratio of fluxes of 100 corresponds to a change in magnitude of exactly 5. Mathematically,

$$m_1 - m_2 = -2.5[\log F_1 - \log F_2] = -2.5\log(\frac{F_1}{F_2}) \tag{1.4}$$

Historically, the star Vega has been used as an arbitrary reference point for fixing our scale, with all stars measured against this zero point. The absolute magnitude, M, is defined as the apparent magnitude of an object if it were 10 parsecs from the Earth. This may be found from the apparent magnitude if the distance (D) to the object is known. This is given by

$$M = m - 5[(\log D) - 1] \tag{1.5}$$

Finally, the bolometric magnitude, M_B, is the total brightness or flux of the object across the entire electromagnetic spectrum, not simply the visual.

1.3.4 Colour

Stars in the night sky appear in a variety of colours to the subjective human eye. In order for colour to have any physical meaning, a proper definition is in order. Astronomers define the colour of an object based on the difference in magnitudes at certain specific wavelengths. For instance, the Sloan Digital Sky Survey (SDSS) make use of five passband filters. These filters block all light except a narrow band with a specific peak wavelength. These are Ultraviolet (u') - 3543Å; Green (g') - 4770Å; Red (r') - 6231Å; Near Infrared (i') - 7625Å; and Infrared (z') - 9134Å. See Figure 1.2.

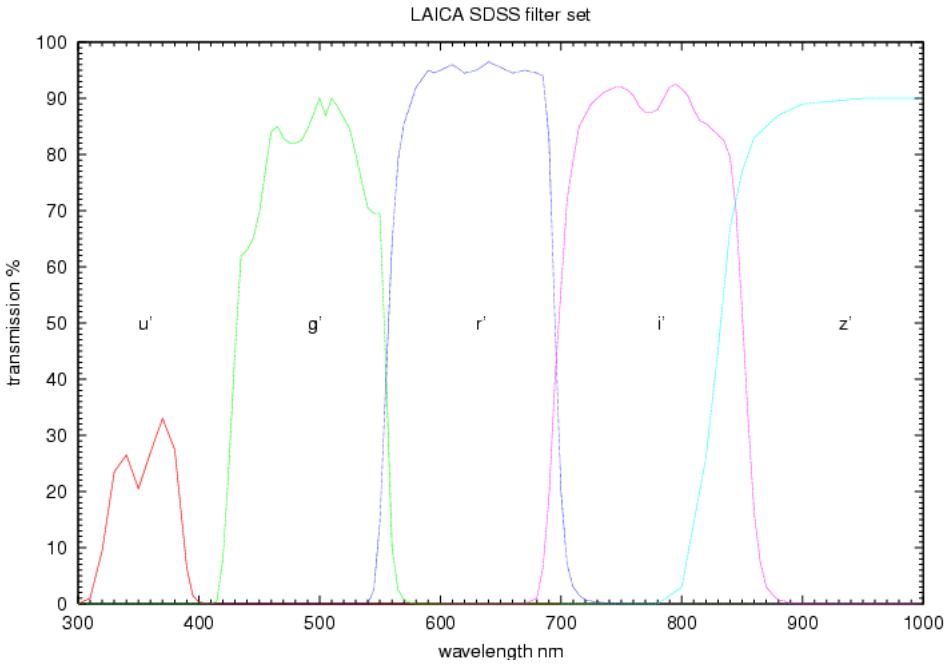

Figure 1.2: A plot showing the band pass intensity curves for the five SDSS filters.

The difference between the magnitudes of light at these specific wavelengths determine the colour of the object. For instance, if a particular star has a $g' - r'$ value of 0.8, then

$$-2.5 \log(\frac{F_{g'}}{F_{r'}}) = 0.8 \tag{1.6}$$

which means that,

$$\frac{F_{g'}}{F_{r'}} = 10^{-\frac{0.8}{2.5}} \tag{1.7}$$

Flipping both sides of the equation we get,

$$\frac{F_{r'}}{F_{g'}} = 10^{0.32} = 2.08 \tag{1.8}$$

In other words, a star with $g' - r' = 0.8$ emits 2.08 times as much red-wavelength light as green-wavelength light.

1.4 Spectroscopy

Our characterisation of hot subdwarfs depends critically on spectroscopic analysis of the light coming from our specimen stars. It is prudent, therefore, to elaborate a little on the process of spectroscopy. All bodies in the Universe radiate electromagnetically. The peak wavelength of this emission depends on the temperature of the body. For a perfect blackbody, this wavelength depends *only* on the temperature. Plotting the intensity of radiation against wavelength gives you the characteristic blackbody curve. Stars approximate very well as a blackbody and as such the spectrum of light emitted will depend only on the atmospheric temperature of the star. Thus, the peak of the spectrum is diagnostic of the star's effective temperature.

If thermal radiation were the only source of light from a star, the star's spectrum would be a smooth curve. However, superimposed upon the spectrum are narrow features called spectral lines. These are caused by the absorption or emission of light of particular wavelengths by the atoms in the outer part of the star. An example is shown in Figure 1.3. It is these features that are unique to each type of star. Indeed, the element helium was first discovered during an eclipse of our Sun in 1868 as a distinctive yellow spectral emission line; the Greek word for our Sun being *helios*.

Depending on the pattern of spectroscopic absorption and emission lines, stars may be grouped into particular spectral types. The traditional spectral types are denoted by the letters O, B, A, F, G, K and M. As the appearance of the various spectral lines depends on the temperature of the star as well as its makeup, this spectral classification

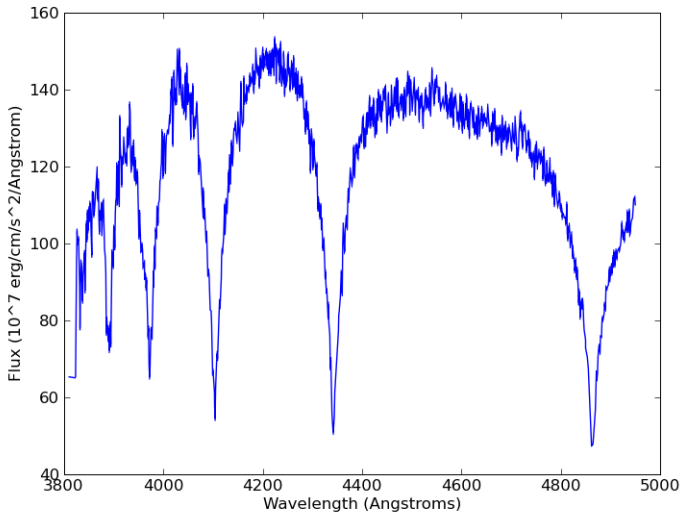

Figure 1.3: An example of an SDSS stellar spectrum, resampled between 3800Å and 4950Å. The hydrogen Balmer absorption lines are evident.

is also a crude temperature scale. O being the hottest, with ionised helium lines and M being the coolest, with strong titanium oxide and sodium lines.

New types of star have been added to the list over the years as our knowledge improved. These include C type carbon-rich stars; smaller, cooler L and T type stars; Wolf-Rayat stars; and of interest in our case, subdwarf stars consisting of sdO, sdB and sdOB spectral types.

1.5 Subdwarf Stars

Subdwarf stars are a band of stars that run underneath the main sequence on a Hertzprung-Russell diagram. They are less massive than our sun and are subluminous in so far as they are 1.5 to 2 magnitudes lower than main sequence stars of the same spectral type.

Subdwarf stars are further subdivided into 'cool subdwarfs' and 'hot subdwarfs'. Cool subdwarfs are main sequence, hydrogen burning stars with low metallicity (that is, fewer elements with Z greater than 2). This lower metallicity decreases the opacity of the outer layers, decreasing radiation pressure and resulting in smaller, hotter stars. Hot subdwarfs, modelled as, and interchangeably termed 'extreme horizontal branch'

stars represent a late stage in the evolution of some stars, and are of interest in this case. Hot subdwarfs are hot, blue stars located to the far left of the Hertzprung-Russell diagram, underneath the main sequence.

There are three broad types of hot subdwarf, although this will be refined a little later. First, sdB stars are a core helium burning star with a very thin hydrogen envelope. They present with strong hydrogen spectral absorption lines. sdOB stars are related to sdBs but potentially contain an inert core. These stars exhibit both hydrogen and helium absorption lines. Finally, sdO stars are precursive to a white dwarf and are hotter as a result. Ionised helium lines are present in the spectra of sdO stars.

There are a number of possible evolutionary tracks for the formation of hot subdwarfs. These include a single star model in which a giant star is stripped of its outer envelope by a stellar wind of some description, leaving behind the helium core. If this ignites, a solitary subdwarf may result (6). The consensus, however, seems to be that most hot subdwarfs form within a binary system. There exist three different channels of formation as a binary: the Common Envelope (CE) Ejection Channel for binaries with short period rotation; Stable Roche Lobe Overflow (RLOF) Channel for binaries with longer period; and the Double Helium White Dwarf (WD) Merger. Some recent computational work by Han et al. (7) has indicated that, of these three formation channels, the CE channel predominates.

We intend to augment our data set of known hot subdwarfs, classify each spectrum according to the scheme laid out in the final chapter and parameterise those spectra in terms of surface gravity, effective temperature and helium abundance in an attempt to further constrain their evolutionary development.

Chapter 2

The Sloan Digital Sky Survey (SDSS)

2.1 What is the SDSS?

The Sloan Digital Sky Survey (or SDSS) is an ambitious astronomical survey designed by a consortium of academic institutions for the express purpose of imaging a large part of the night sky with a view to obtaining redshift data from stars, galaxies and quasars, numbering in the millions, for the eventual purpose of constructing a 3 dimensional map of our Universe. A valuable byproduct of this endeavour is access to a huge number of photometric and spectroscopic measurements that lend themselves quite easily to alternative analysis.

2.2 SDSS Instrumentation

The SDSS uses a dedicated 2.5m telescope on Apache Point in Sunspot, New Mexico. The telescope is equipped with a 120-megapixel camera, essentially a network of thirty CCDs, capable of imaging 1.5 square degrees at a time, about eight times the area of the full moon. The photometric system employs five well-defined, passband filters - Ultraviolet (u'), Green (g'), Red (r'), Near Infrared (i') and Infrared (z'). In addition to the main telescope, a 0.5m secondary telescope is used to monitor subtle changes in atmospheric conditions allowing corrections to be made to the measurements obtained with the main telescope. Additionally, a pair of spectrographs can isolate and examine the spectra from up to $5,000$ individual stars or galaxies at any one time using specially designed aluminium plates. The spectrographs split the light from each object into

composite wavelengths spanning 3800Åto 9200Å. Finally, the telescope is serviced by a custom-designed set of software pipelines capable of keeping pace with the enormous flow of data from the telescope, about 200GB per night.

2.3 Observational process

The SDSS telescope uses a drift scanning technique which allows the telescope to remain fixed while making use of the Earth's rotation to record strips of the night sky. In June 2005, the SDSS completed the first phase of operations - SDSS-I. This survey covered over $8,000$ square degrees of the sky, detecting nearly 200 million celestial objects and measuring the spectra from more than $675,000$ galaxies, $90,000$ quasars and $185,000$ stars. The newest phase of operations - SDSS-II - commenced subsequently. SDSS-II has carried out three distinct surveys - the Sloan Legacy Survey, a further examination of the large scale structure of the Universe; SEGUE, an exploration of our own Galaxy, the Milky Way; and the Sloan Supernova Survey. An amalgamation of data from SDSS-I and all projects associated with SDSS-II was released under Data Release 7 (DR7), the source of all of the data included here.

The SDSS database may be used to search for the spectra of hot subdwarfs which can then be analysed using the techniques outlined in the following chapter.

Chapter 3

Computational Methods

Initially, query parameters may be used to narrow our data somewhat to objects of a particular colour - blue stars in this case. This is outlined in more detail in the subsequent section on the application of the following computational techniques to our SDSS data. Once this download is complete, there are three main computational techniques used to filter this large database for hot subdwarfs and subsequent analysis of these spectra. Filtering for particular types of objects from a large database is a difficult task. This is accomplished using Principal Component Analysis (PCA), described below. Classification of our spectra is carried out using an Artificial Neural Network (ANN), which is described in the second section and finally, parameterisation of the spectra can be done using a χ^2 fitting technique outlined briefly in the final section.

3.1 Principal Component Analysis

Principal Component Analysis (PCA) is a statistical technique used to extract the main sources of linear variation within a data set. Initially introduced by Pearson (8) and independently by Hotelling (9), it is essentially a vector space transform used to reduce multidimensional data sets to a handful of independent parameters that capture the main sources of variation. In this case, we can use it to examine the defining features from a set of known hot subdwarf spectra, those belonging to Drilling et al. (10). These features can then be used to determine if an unknown spectrum is similar to our original archetype and thus allow for speedy filtration.

3.1.1 Mathematics of PCA

This presentation follows that of Murtagh and Heck (1987)(11). Let the vector $\mathbf{x} = (x_1, x_2, ..., x_N)$ be a stellar spectrum with N flux bins. A spectrum can then be considered as a point in N-dimensional space, with each axis representing each flux bin. M such spectra may be described as the $(M \times N)$ transposed matrix $\mathbf{X}^T = (\mathbf{x}_1, \mathbf{x}_2, ..., \mathbf{x}_M)$.

The first principal component is the normalised vector, $\mathbf{u}$, which best fits the points in $\mathbf{X}^T$. The criterion of goodness of fit of this axis to the point set is defined as the squared deviation of the points from the axis. Minimising the sum of distances between the points and the axis is equivalent to maximising the sum of squared projections onto the axis, i.e. maximising the variance of the points when projected onto this axis. The sum of squared projections of the points in $\mathbf{X}^T$ onto the new axis, $\mathbf{u}$, is

$$(\mathbf{Xu})^T (\mathbf{Xu}) \tag{3.1}$$

In maximising this quadratic form, the constraint must be made that $\mathbf{u}^T \mathbf{u} = 1$, otherwise the projection can be maximised arbitrarily. Setting $\mathbf{S} = \mathbf{X}^T\mathbf{X}$, and introducing the Lagrange multiplier, λ, the maximum is obtained by differentiating

$$\mathbf{u}^T\mathbf{Su} - \lambda(\mathbf{u}^T\mathbf{u} - 1) \tag{3.2}$$

which gives,

$$2\mathbf{Su} - 2\lambda\mathbf{u} \tag{3.3}$$

Setting this equal to zero, the optimal value of $\mathbf{u}$ is the solution of

$$\mathbf{Su} = \lambda\mathbf{u} \tag{3.4}$$

This is a standard eigenvector problem. The eigenvector of $\mathbf{S}$, $\mathbf{u}$, is the line of best fit, and corresponding eigenvalue, λ, indicates the amount of variance described by this line. Calculating the remaining axes proceeds in a similar manner, with the additional constraint that each new axis be perpendicular to the last. In this way, we can determine the principal components of our data set.

3.1.2 Building a hot subdwarf filter

Our intent is to perform Principal Component Analysis on a set of known hot subdwarf spectra with a view to extracting the main sources of variation. By retaining only the most significant principal components from our N-dimensional data set, a quick test can determine if a new data point is in a similar region of N-dimensional space as the original data set.

3.2 Artificial Neural Network

Classification of our spectra is carried out using an Artificial Neural Network (ANN). We make use of the ANN code STATNET from Bailer-Jones (1996) (12).

An artificial neural network is a machine learning algorithm which is modeled from the network of neurons forming the biological central nervous system and were introduced in a simplified form by McCulloch and Pitts (13) in 1943. Much is still unknown about the nervous system, but what we do know is equally intriguing. The brain and extended nervous system is basically a large signal processor, typically containing 10^9 neurons, with an average of several thousand interconnections per neuron. While there are many different types of biological neuron, each neuron has four major components - the dendrites (input structure), the cell body (signal processor), the axon (output structure) and the synapses (the link between the axon of one neuron and the dendrites of another). Electrical signals are collected by each individual neuron through the dendrites, a host of long, thin structures. This signal is then passed to the cell body which activates only if the input signal exceeds a certain threshold (the firing threshold). It appears as though all of the signals sent from neuron to neuron are identical. The key to the whole process lies in the strength of the signal received by a neuron, which critically depends on the efficacy of the synapses, the connection between neighbouring neurons, as each synapse is 'weighted' differently. Therefore, the brain appears to interpret different information based upon the path taken by the signal, which depends entirely on synaptic performance. While this is an accurate account of modern neuroscience, in its broadest sense, some of the details are still in debate and much is not fully understood. However, it is not necessary to understand brain function in detail in order to comprehend the function of an artificial neural network. It is remarkable that such interestingly complex behavior can be achieved using a model not much more complicated than that outlined above.

When creating a functional model of the biological network, there are three basic components of great importance. First, the synapses of the neuron are modeled as weights. The strength of the connection is noted by the value of the weight. Negative weight values reflect inhibitory connections, which have their parallel in inhibitory neurons in the brain; positive weight values designate excitatory connections. The next two components model the actual activity within the neuron cell. A summing junction takes the place of the cell body whose function is to sum the various inputs modified by their respective weights. This result is a linear or a non-linear combination of inputs, as desired. In our case, we will make use of a non-linear combination of inputs. If we take x as the input and y as output, then the function is determined from the coefficients $w_0, ..., w_n$, which are analogous to the weights associated with each biological synapse, as follows.

$$y(x) = w_0 + w_1 x + ... + w_n x^n = \sum_{i=0}^{n} w_i x^i \tag{3.5}$$

The weights can be determined by means of error minimisation between the desired output from the polynomial, $d(x_k)$, for each input value, x_k, and the actual output of the polynomial, $y(x_k)$. In this way, the ANN can be taught a given classification scheme by iterative approximation during a period of *supervised training* with a set of known spectra. There is a well-documented trade off between over-fitting the training data and the ability to generalise to a new set of data. The ideal balance occurs when the number of degrees of freedom in the model is relatively small compared to the size of the training data set. A more detailed account can be found in Bishop (1995) (14).

Our spectra are confined to the wavelength region 4050Å to 4900Å, at a resolution of 2.5Å and our classification consists of a 'spectral' type, 'luminosity' class and 'helium' class.

3.3 χ^2 Fitting

Parameterisation was achieved using SFIT2, a modification to SFIT, a χ^2 fitting algorithm developed by Jeffery and altered significantly by Winter, both at Armagh Observatory (1). SFIT2 searches a grid of theoretical model spectra to find the combination of physical parameters which most closely matches an observed spectrum. The main improvements on the original program include increased flexibility with regard to grid size and a less sensitive interpolation scheme for approximating the space between grid points.

Once a match has been made between our input spectrum and a model spectrum, we can infer the astrophysical parameters of interest - in this case $\log g$, effective temperature and helium abundance.

If we once again let $\mathbf{x} = (x_1, x_2, ..., x_N)$ be the spectrum we wish to parameterise, and $\mathbf{s} = (s_1, s_2, ..., s_N)$ be a template spectrum with known physical parameters. The distance metric to be minimised is of the form

$$D = \frac{1}{N}\left[\sum_{i=1}^{N} w_i |x_i - s_i|^p\right]^{\frac{1}{p}} \tag{3.6}$$

where w_i is a weight assigned to flux element s_i of the template spectrum. Typically, $\mathbf{s}$, is only one template in a set, $\mathbf{S} = (\mathbf{s}_1, \mathbf{s}_2, ..., \mathbf{s}_M)$, and D is computed for all templates $\mathbf{s}_j$. This process becomes χ^2 fitting when $p = 2$ and $w_i = \sigma_i^{-2}$, where σ_i is the error in x_i.

Chapter 4

Application to SDSS Hot Subdwarfs

Having established our set of automatic analysis techniques, these can now be applied in the case of hot subdwarf stars from the SDSS. Firstly, our search of the SDSS archive is narrowed by devising a set of criteria based on photometric colours. The data is filtered further using PCA, before being fed to the analysis pipeline for classification and parameterisation.

4.1 Search Criteria

Following the work of Harris et al. (2003) (15) and Kleinman et al. (2004) (16) a search of the SDSS archive was carried out which was based on the *u'g'r'i'z'* point spread function colour magnitudes. An additional constraint is permitted if we decline those spectra which have been classified as a quasar by the SDSS (these stars are given the SDSS Spectral Classification 'QSO'). This was achieved using Structured Query Language (SQL), as outlined below.

```
SELECT s.plate, s.mjd, s.fiberID
FROM BESTDR7..SpecPhoto as s
WHERE s.psfMag_u < 21
AND (s.psfMag_u - s.psfMag_g) < 0.7
AND (s.psfMag_g - s.psfMag_r) < -0.1
AND s.specClass  <>  dbo.fSpecClass ('QSO')
```

The total quantity of spectra retrieved was 11,999. These spectra will include unwanted Blue Horizontal Branch (BHB) stars and White Dwarfs (WDs) which are both of similar photometric colour. It is these stars we wish to filter from the desired hot subdwarfs.

4.2 Filtering

First, we must construct a filter using spectra from a known set of hot subdwarfs. Choosing to narrow our wavelength range from 4050Å to 4950Å we use PCA to analyse a collection of 177 spectra from subdwarfs and blue horizontal branch stars made available by Drilling et al. (10). It was discovered that the hydrogen and helium spectral absorption lines were the diagnostic feature of interest representing the first two principal components and accounting for 98% of the variance within the data set. The first principal component is shown in Figure 4.1. The PCs are rotations in the data space of the original axes, and therefore resemble spectra.

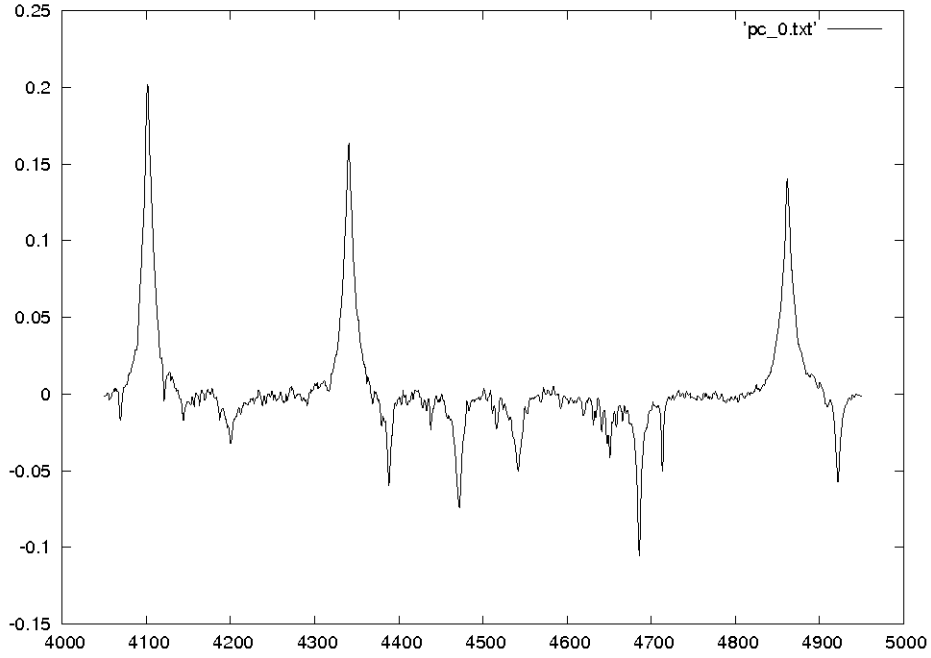

Figure 4.1: The first Principal Component of the Drilling et al. (10) sample. These are the three hydrogen Balmer lines: $H\beta$, $H\gamma$ and $H\delta$.

Accepting just the first four PCs, we account for 99.3% of the variation and this is more than adaquate to give a compressed representation of the Drilling et al. (10) hot subdwarf standards.

Taking our 11,999 spectra, the SDSS-normalised spectrum was extracted from each of the downloaded FITS files, and velocity corrected using the SDSS-derived redshift stored in each FITS file header. We then proceeded to filter these spectra. Our PCA filter keeps only those spectra that are arbitrarily similar to our archetype. This is determined by our threshold PCA RMS value, which we initially set at 2.5. The result after filtering was 2,775 spectra. Reducing the RMS value to 1.5, and thereby accepting only those spectra with a good S/N ratio, equivalent to excluding longer distance stars, we are left with 794 potential hot subdwarf spectra, although these will almost certainly contain some unwanted spectra.

4.3 Analysis

The SDSS-normalised spectra were created by fitting a pseudo-continuum using a median/mean filter. However, this pseudo-continuum tends to underfit the real continuum for the higher order Balmer lines, and while this is sufficient for filtering purposes, it cannot be used for classification or parameterisation. Instead, our hot subdwarf spectra were normalised using an automated method based on cubic spline fitting. Each sample is then resampled onto the common wavelength grid of 4050Å to 4950Å at a sampling rate of $1\text{Å}\,\text{pixel}^{-1}$.

4.3.1 Classification

The next step is to classify our stars spectroscopically, and according to an extension of the so-called MK classification system, see Table 4.1. This classification depends on spectral lines sensitive to stellar surface gravity, which is related to luminosity. The scale uses a spectral type running from sd01 to sdA $(1-20)$, analagous to MK spectral classes. It introduces a helium class $(0-40)$ based on H, HeI and HeII line strengths and assigns luminosity classes I - IX, where most subdwarfs have luminosity class VII.

We wish to assign a spectral type, luminosity class and helium class to each spectrum.

Classification may be carried out using an Artificial Neural Network (ANN). Once again, we make use of a known set of hot subdwarf spectra which have already been classified by eye according to the classification scheme outlined above. During a period of *supervised training* the ANN learns the same classification scheme and can then be used to classify our set of SDSS spectra accordingly. The results are outlined in

Table 4.1: Range of Classification

Spectral Type	Luminosity Class	Helium Class
O1	0	0
O2	I	...
O3	II	10
...	III	...
O9	IV	20
B0	V	...
B1	VI	30
B2	VII	...
...	VIII	40
A	IX	

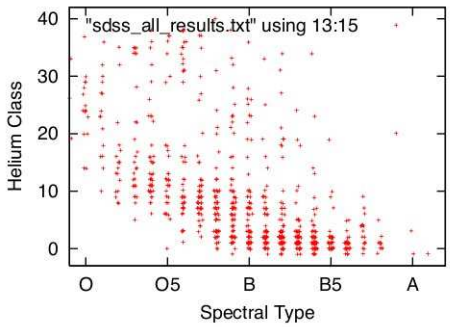

Figure 4.2: A plot of Helium Class against Spectral Type. For clarity, points have been offset by small random shifts in both coordinates.

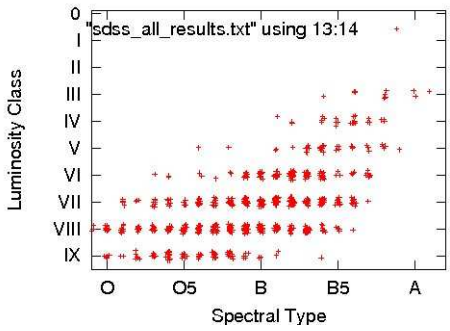

Figure 4.3: A plot of Luminosity Class against Spectral Type. For clarity, points have been offset by small random shifts in both coordinates.

Figures 4.2 to 4.4. These relationships serve to demonstrate some of the obvious broad correlations, such as luminosity class and spectral type.

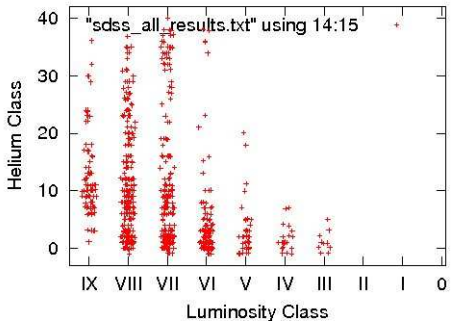

Figure 4.4: A plot of Helium Class against Luminosity Class. For clarity, points have been offset by small random shifts in both coordinates.

4.3.2 Paramaterisation

Physical parameters in $T_{\rm eff}$, $\log g$, and $\log(n_{\rm He}/n_{\rm H})$ were derived by fitting each spectrum to a large grid of 2426 Local Thermal Equilibrium (LTE) model spectra generated using STERNE and SPECTRUM, and outlined in the Table 4.2.

Table 4.2: LTE Model Grid

Parameter	Values
$T_{\rm eff}$ (kK)	8.0, 9.0, 10.0, 12.0, 14.0, 15.0, 16.0, 18.0, 20.0, 22.0, 24.0, 25.0, 26.0, 28.0, 30.0, 32.0, 34.0, 35.0, 36.0, 38.0, 40.0, 45.0, 50.0
$\log g$	2.50, 3.00, 3.50, 4.00, 4.50, 5.00, 5.50, 6.00
$n_{\rm He}$	0.001, 0.01, 0.05, 0.1, 0.3, 0.5, 0.7, 0.9, 0.95, 0.99, 0.999

The results of parameterisation are presented in Figures 4.5 and 4.6. A number of interesting features present themselves in our plot of surface gravity against effective temperature, in Figure 4.5. There are two broad trends, one that stretches from high surface gravity, high effective temperature at the bottom left up to $\log g = 3.5$, low effective temperature. The other stretching from $T_{\rm eff} = 25\,000K$, $\log g = 3$ to low surface gravity, high effective temperature at the top left. The hotter sdO stars lie along a stretch of points to the left of, and parallel to, the numerous sdB stars. It can be seen that our filtering for hot subdwarfs has not been perfect, included in our data are BHB stars and post-AGB stars, some with remarkably low surface gravity and high effective temperature. Within the sdB sequence there appears to be two alternative trends (labelled 1 and 2), hinting at distinct formation alternatives. There is, in addition, a low density region centred around $T_{\rm eff} = 22\,000K$. This same low density region was observed by Green et al. (2006) (17) and others, although it is significantly more populated than expected. This low density area lies between our hot subdwarfs and

the blue horizontal branch stars and probably reflects differing evolutionary processes. An anomalous feature in Figure 4.5 are the clumping of stars into small groups and along lines of constant $\log g$. This is no doubt due to holes in the model grid and the tendency of the parameterisation to overfit the surface gravity.

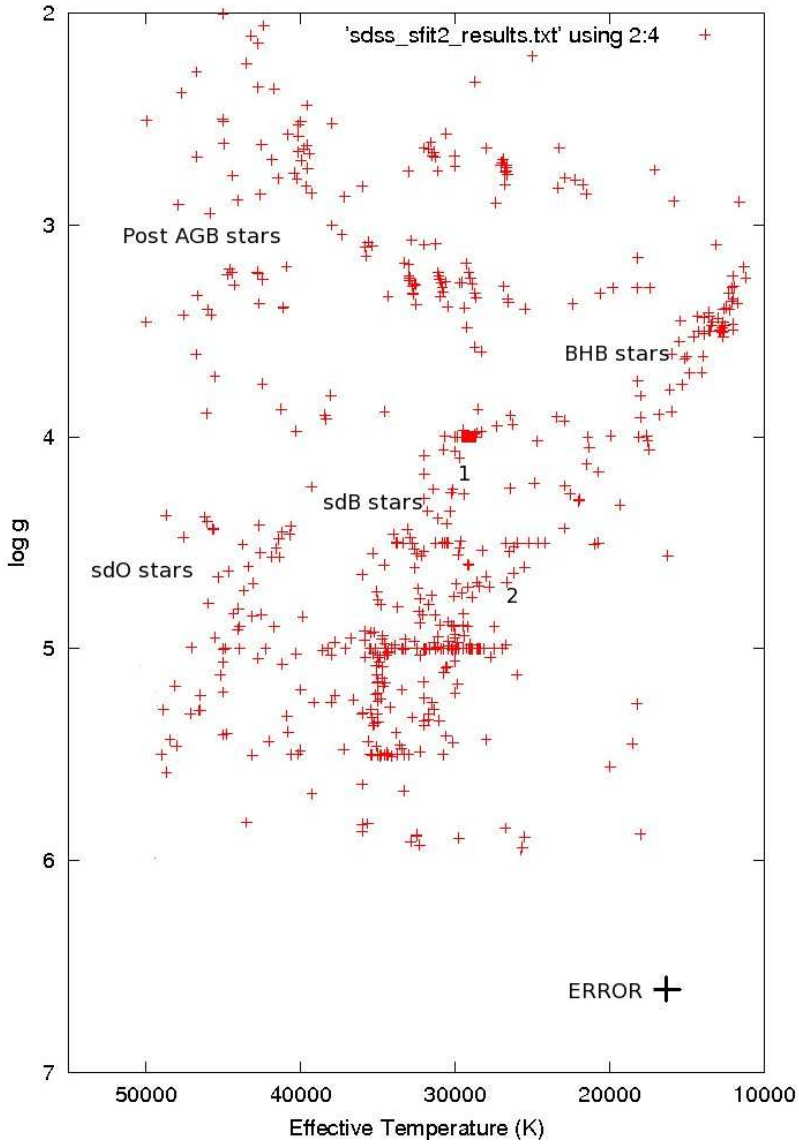

Figure 4.5: A plot of Surface Gravity against Effective Temperature.

In Figure 4.6 there are two regions of note, hydrogen rich sdB stars at the bottom right and helium rich sdO stars in the top left. There are a few extreme helium rich stars at the very top of our plot.

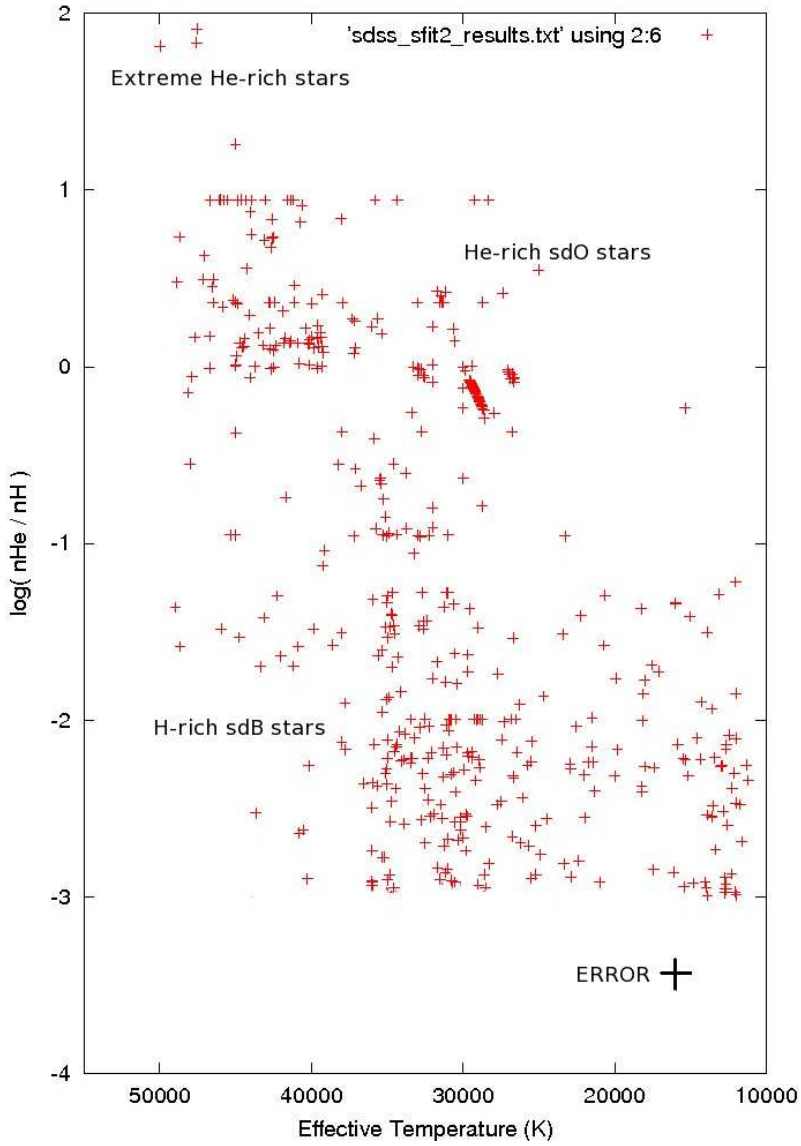

Figure 4.6: A plot of Helium Abundance against Effective Temperature.

Our analysis of hot subdwarf spectra allows us to examine the correlation between their various stellar parameters in order to better understand their evolutionary development. In both Figure 4.5 and 4.6, it is clear that despite very broad trends, there is significant non-uniform distribution. This should be expected given the various evolutionary channels mentioned in Section 1.5.

4.4 Error Analysis

There are several sources of error throughout the analysis process. In terms of pre-processing, the normalisation of our spectra presents a significant problem, causing some slight anomalies. The training process associated with the artificial neural network involves a trade off between overfitting of the training sample and ability to generalise in the face of new data and as such the spectral classification is not perfect. Lastly, the ability of our χ^2 fitting varies from spectrum to spectrum and provides only a closest match. The models used in the parameterisation process assume a stellar atmosphere that is in local thermal, radiative and hydrostatic equilibrium. The error that appears in the parameterisation plots is the average variance between the model and the spectra. Discussion of errors arising from these computational methods is a complicated and intricate problem, beyond the scope of this report.

Chapter 5

Conclusion

Our initial aim with this project was to source new hot subdwarf spectra, and to analyse these spectra using a set of automated techniques with a view to improving our knowledge regarding the evolution of these unusual stars. To this end a request was made to the Sloan Digital Sky Survey (SDSS) for all blue stars not already classed as a quasar by the SDSS team. Filtering was then necessary in order to reduce our set of blue stars solely to hot subdwarfs. Once this was achieved, we set about classifying and parameterising these hot subdwarf spectra. Our main results may be summarised as follows:

1. Higher population within the low density area of Green et al. (17), centred at $T_{\text{eff}} = 22\,000K$ inside the $\log g$ - T_{eff} plot, delineating between sdB stars and BHBs.
2. Double banded sdB sequence within our $\log g$ - T_{eff} plot.
3. Two helium abundance sequences within the $\log(n_{\text{He}}/n_{\text{H}})$ - T_{eff} plot.

Time constraints prevented further examination of our results. There is scope for an increase in the spectral range of our hot subdwarf spectra for inclusion in our PCA filtering. This might serve to exclude more of the unwanted spectra. This could also be achieved by manual investigation of the surviving spectra after the filtering process. Enlarging and improving our model grid for use with our χ^2 parameterisation would help to reduce error and prevent some of the statistical artefacts. Analysis of our data in 3 dimensional parameter space encompassing $\log g$, T_{eff}, and $\log(n_{\text{He}}/n_{\text{H}})$ would also provide further insight.

Bibliography

Winter, C., *On the automatic analysis of stellar spectra*, PhD Thesis, Armagh Observatory, Armagh, 2006.

Smith, M.D., *The origin of stars*, P 222, Imperial College Press, 2004.

Schutz, B., *Gravity from the ground up*, Cambridge University Press, Cambridge, UK, 2003.

Gray, D.F., *The observation and analysis of stellar photospheres*, Cambridge University Press, Cambridge, UK, 1992.

Jeffery, C.S., *Stellar Structure and Evolution: An Introduction*, Course Notes, 2007.

Lee, Y. W., Astrophysical Journal, 430, L113 1994.

Han, Z. et al., *The origin of subdwarf B stars - II*, Mon. Not. R. Astron. Soc., 341, 669691, 2003.

Pearson, K., *On lines and planes of closest fit to systems of points in space*, Philosophical Magazine, 2, 559-572 1901.

Hotelling, H., *Analysis of a complex of statistical variables into principal components*, Journal of Educational Psychology, 24, 417-441. 1933.

Drilling, J. S., Jeffery, C. S. et al., in Preparation, 2006.

Murtagh, F. & Heck, A., *Multivariate Data Analysis*, D. Reidel Publishing Co., 1987.

Bailer-Jones, C.A.L., *PhD Thesis*, University of Cambridge, 1996.

McCulloch, W.S., Pitts, W., *A logical calculus of the ideas immanent in nervous activity*, Bull. Math. Phys. 5 (1943) 115-133.

Bishop C.M., *Neural Networks for Pattern Recognition*, Oxford University Press, Oxford, UK, 1995.

Harris, H.C. et al., AJ 126, 1023, 2003.

Kleinman, S.J. et al., ApJ 607, 426, 2004.

Green, E. M., Fontaine, G. et al., Ed. R. H. Ostensen, *Proceedings of the 2nd Meeting on Hot Subdwarfs and Related Objects*, Baltic Astronomy, Vol. 15, Nos. 1-2, 167-174, 2006.

Clayton, D.D., *Principles of stellar evolution and nucleosynthesis*, University of Chicago Press, Chicago, USA, 1983.

Heber, U., Jeffery, C.S. (Eds.), *The atmospheres of early-type stars, Proceedings, Kiel, Germany*, Springer-Verlag, 1992.